Interfacial gravity currents. II. Wave excitation

A. P. Mehta, B. R. Sutherland,[a] and P. J. Kyba
Department of Mathematical Sciences, University of Alberta, Edmonton, Alberta T6G 2G1, Canada

(Received 28 June 2000; accepted 9 July 2002; published 5 September 2002)

We examine the response of a two- and three-layer salt-stratified fluid to the collapse of a mixed region intruding along the middle layer. For sufficiently deep middle layers, the intrusion (an interfacial gravity current) excites a double-humped solitary wave appearing in the interfacial layer in front of the intrusion head. When the solitary wave is generated the current stops propagating. Trailing the intrusion are large-amplitude trapped internal waves. We study the effect of middle-layer depth and density difference to determine the conditions under which a solitary wave is generated. We propose that this transition occurs because the intrusion resonantly couples with trapped internal waves for a sufficiently thick interface. © *2002 American Institute of Physics.* [DOI: 10.1063/1.1503355]

I. INTRODUCTION

A gravity current (also known as a density or buoyancy current) is an intrusion that moves under the influence of gravity when a fluid of one density propagates horizontally into an ambient fluid of another density. Some examples of gravity currents in the atmosphere are sea-breeze fronts,[1] microbursts,[2] and other manifestations of thunderstorm outflows. A recent summary of observations and experiments of gravity currents has been given by Simpson.[3]

There have been numerous experimental and theoretical studies of the dynamics of gravity currents intruding into a uniform environment.[4–8] Gravity currents are closely related to turbulent bores, phenomena in which the depth of fluid increases as it passes through a hydraulic jump. In a two-layer fluid the bore is turbulent if the ratio of the depth of the fluid behind and ahead of the bore approximately exceeds 4 (e.g., see Ref. 3, Sec. 13). A gravity current occurs if the depth of the fluid ahead of the bore is negligibly small. In the opposite limit, where the ratio of the depths is close to unity, an undular bore develops. The formation and characteristics of such internal bores have been studied both experimentally and theoretically.[9–11] Similar to and sometimes identified with undular bores are solitary waves. These are hump-shaped disturbances that displace mass a finite distance. Unlike undular bores, the fluid depths behind and ahead of a solitary wave are the same. The structure and speed of internal solitary waves has been well studied in theory[12–16] and experiments.[17–20]

When a gravity current propagates in a stratified ambient fluid, bores, internal waves, and internal solitary waves may be generated. The conditions under which a bottom-propagating gravity current may create a bore in a two-layer fluid have been studied experimentally by Rottman and Simpson.[21] They observed a bore propagating ahead of the gravity current under ''partial blocking'' conditions.[9,10] In attempts to create complete blocking conditions, the gravity current instead propagated along the interface between the two layers of the ambient fluid.

The dynamics of intrusions along the interface of a two-layer fluid have been examined in a variety of experiments.[22–24] In particular, Maxworthy[23] investigated the behavior of solitary waves excited by an intrusion in a two-layer fluid with a ''thick'' (molecularly diffused) interface. Noh *et al.*[25] observed solitary waves generated by an intrusive fluid (a ''thermal'') propagating along a density interface. In a study of an intrusion in more complex stratification, Manasseh *et al.*[26] examined the propagation of a thermal incident upon a linearly stratified lower layer. They observed a solitary wave developing over the thermal, which in turn lost mass and stopped propagating.

As a step toward understanding the dynamics of a gravity current in a continuously stratified system, it is useful to determine the various wave behaviors in a three-layer fluid. Because of its relatively simple structure experimental results may be compared with analytic theories. A three-layer fluid introduces dynamics not present in a two-layer fluid because of the more complex dispersion relation of internal waves. In a companion paper,[27] a three-layer fluid has been shown to develop naturally due to interfacial mixing by the passage of successive intrusions. In the experiments discussed here the ambient fluid is initially a three-layer fluid, and the analyses focus upon the excitation of waves from the intrusion.

We examine the behavior of the flow within a salt-stratified fluid by way of lock-release experiments. The ambient fluid structure is symmetric: the lower and upper layers are of equal depth and, in three-layer fluid experiments, the density of the middle layer is the average of the outer two layers. If the width of the middle layer exceeds a critical depth, an intrusive gravity current is found to excite an internal ''double-humped'' solitary wave in front of the gravity current head. The wave is double-humped or (using the language of internal waves in three-layer fluids) varicose in the sense that the wave crest on the upper interface of the middle layer overlies and, indeed, is coupled to the wave trough on

[a]Author to whom correspondence should be addressed. Electronic mail: bruce.sutherland@ualberta.ca

the lower interface. As the solitary wave is generated the current itself stops propagating. Trailing the gravity current are large-amplitude trapped internal waves.

In the language of solitary wave theory, this sequence of events may alternately be described as the transition from a large-amplitude solitary wave with closed streamlines (which therefore transports mass within the streamlines along with the wave) to a smaller amplitude solitary wave with open streamlines (which displaces but does not transport mass long distances). We choose not to adopt this terminology because of the ambiguity introduced when examining the transition from two- to three-layer fluid dynamics. In a two-layer fluid, the phenomena is best described as an intrusive gravity current, not a solitary wave with closed streamlines, because the middle-layer interface increases from zero ahead of the intrusion to finite depth behind the intrusion and because a double-humped solitary wave with open streamlines cannot occur in this case. Thus, to be consistent, for both two- and three-layer fluid experiments we describe the phenomena that transports the mass long distances from the lock as an intrusion.

The experimental setup and qualitative results are described in Sec. II. In Sec. III we extend the predictions of shallow water theory to a three-layer fluid and we derive estimates of momentum transport associated with intrusions and waves. Theories and experimental results are compared in Sec. IV and concluding remarks are given in Sec. V.

II. EXPERIMENTAL SET UP

Experiments of intrusions in two- and three-layer fluids have been carried out in which the relative densities of the layers and the thickness of the middle layer are varied.

The experiments are performed in a glass tank measuring 197.3 cm long, 17.3 cm wide, and 48.5 cm tall. In the special case of a two-layer fluid, salt water of density ρ_1 is filled to a depth of 9 cm in the tank. A 9 cm deep layer of fresh water, of density ρ_0, is layered on top by adding the water through a sponge float. The total depth of the fluid is $H=18$ cm. The density difference between the two layers is denoted by $\Delta\rho=\rho_1-\rho_0$. In setting up a three-layer experiment with a middle-layer depth of d, the bottom layer is filled with salt water of density ρ_1 to a depth $(H-d)/2$. A weaker salt water solution of density $\rho_m=\frac{1}{2}(\rho_0+\rho_1)$ is layered on top through a sponge float until the total fluid depth is $(H+d)/2$. Finally fresh water is layered on top until the total depth of stratified fluid in the tank is H. In each experiment, $H=18$ cm and the upper and lower layers have equal depth. In some experiments the density profile is not determined explicitly. The density of the three layers and the middle layer width are estimated from the conditions used to set up the experiments. Typically, $d=0$, 2, 3, and 4 cm. In experiments used to measure the speed of intrusions and waves, a traversing conductivity probe is used to measure density profiles.[27]

A water-tight gate is inserted 8.4 cm from one end of the tank between two 1 mm thin glass strips forming a vertical guide from which the gate can be rapidly extracted. The fluid behind the gate is thoroughly mixed to create a homogeneous fluid with density approximately equal to ρ_m. This mixed fluid is dyed so that it can be easily distinguished from the ambient fluid after the gate is removed. When the fluid in the lock is almost stationary the gate is rapidly extracted. The lock fluid then collapses to form an intrusion along the interface at mid-depth.

In some experiments with $d=0$ and 2 cm, intrusions are successively released throughout a number of runs. The mixing caused by the intrusions acts to widen the middle layer.

To analyze the characteristics of the intrusions and interfacial waves, the experiments are recorded on a digital video camera focusing on a 20 cm wide window of the tank extending between 80 and 100 cm from the lock-end of the tank. The DigImage software package[28] is used to take velocity, wavelength, amplitude, and other measurements determined from digitized time-series images. Accurate measurements of intrusion and wave speeds are determined from images extending over the full length of the tank.

If the middle-layer depth is less than 2 cm, the intrusion propagates along the middle layer to the end of the tank. Kelvin–Helmholtz instabilities are observed behind the head. The development of the instabilities becomes less pronounced if the middle-layer depth is larger than 2 cm. This relation between the instability size and interface width has also been observed by Britter and Simpson[24] in their two-layer experiments. We also observe that the Kelvin–Helmholtz billows appearing behind the intrusion head increase in size for a faster intrusion (larger $\Delta\rho$). This occurs because there is greater velocity shear at the interface between the head and the ambient fluid.[5,29]

In the case of a two-layer fluid, the trapped internal waves behind the intrusion are of small amplitude and persist for one or two wavelengths. If the middle layer is sufficiently wide, a double-humped solitary wave is excited in the interfacial layer propagating in front of the intrusion head. Upon the creation of the solitary wave the intrusion stops propagating. Trailing the intrusion are large-amplitude quasi-monochromatic internal waves. Figure 1 shows a schematic illustrating this transition.

III. THEORY

The experiments show that the dominant flow is spanwise-uniform across the width of the tank. Therefore, the relevant dynamics can be described by a theory for two-dimensional flow. We examine the predictions of simple two- and three-layer models in order to develop insight into the dynamics of trapped internal waves, gravity currents, and solitary waves in a three-layer fluid.

A. Intrusive gravity current speed

The steady-state speed of a bottom-propagating dissipative gravity current of density ρ_m intruding into a finite-depth fluid of density ρ_0 was predicted theoretically by Benjamin.[5] In good agreement with experiments,[30] he found the propagation speed, u_{gc2}, to be given by

$$\frac{u_{gc2}^2}{g_2'\Delta d_2}=\frac{(H_2-\Delta d_2)(2H_2-\Delta d_2)}{H_2(H_2+\Delta d_2)}, \tag{1}$$

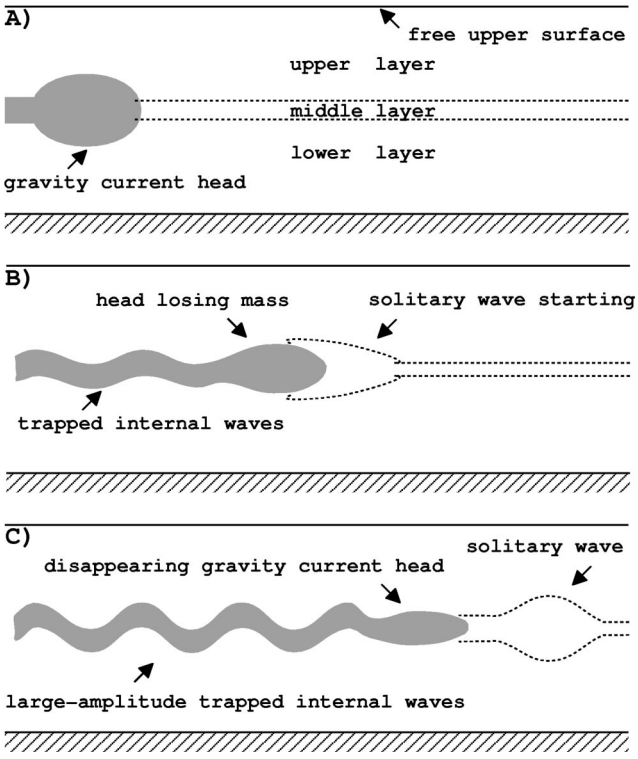

FIG. 1. Schematic showing the excitation of internal waves and solitary waves during the collapse of an interfacial gravity current.

in which H_2 is the depth of the fluid into which the gravity current intrudes and Δd_2 is the depth of the tail sufficiently far behind the gravity current head. The reduced gravity $g_2' = g(\rho_m - \rho_0)/\rho_m$ is given in terms of the density difference between the gravity current and the ambient.

Symmetry arguments may be used to extend this theory to predict the speed, u_{gc3}, of an intrusion along the interface of a two-layer fluid. For ease of interpreting the discussion below, a schematic of an intrusion in a three-layer fluid is shown in Fig. 2. The total fluid depth is H and it is assumed the upper and lower layers each have depth $H/2$. The total depth of the tail of the intrusion sufficiently far behind the head is Δd. Setting $H_2 = H/2$ and $\Delta d_2 = \Delta d/2$, and using the relation $\rho_m - \rho_0 = \Delta\rho/2$, (1) gives

$$\frac{u_{gc3}^2}{g\sigma\Delta d} = \frac{1}{4}\frac{(H-\Delta d)(2H-\Delta d)}{H(H+\Delta d)}. \tag{2}$$

In this expression, the relative density difference, σ, is defined by

$$\sigma \equiv \frac{\Delta\rho}{\rho_m} = \frac{\rho_1 - \rho_0}{\rho_m}. \tag{3}$$

The speed, C_{gc}, of an intrusion in an infinitely deep fluid is given by (2) in the limit $H \to \infty$:

$$C_{gc} = \sqrt{g\sigma\Delta d/2}. \tag{4}$$

In deriving (2) and (4), it is assumed the thicknesses of the interfaces are negligibly small. However, in experiments of intrusions into a two-layer fluid the width of the tail behind the intrusion is comparable with the initial interface thickness.[27] Both are on the order 0.5–1.0 cm. Thus some discrepancies with theory are anticipated. The theory furthermore assumes there are no waves trailing behind the intrusion head.

In an internal bore, a two-layer fluid undergoes a hydraulic jump so that the ratio of the lower to upper layer depths changes to a new, but constant value. In the notation of a gravity current above, assuming the total depth, H_2, of the fluid is constant, the lower layer depth is taken to jump from a depth of d_2 to $d_2' \equiv d_2 + \Delta d_2$ during the passage of the bore. A bottom-propagating gravity current is a limiting case of a bore where d_2 is zero. Internal bore speeds have been predicted by Yih and Guha[31] and Wood and Simpson,[10] but these are not consistent with (1) in the limit $d_2 \to 0$. Rather than assuming energy losses occurred within a bottom-propagating bore, Klemp *et al.*[11] assumed that energy losses occur within the upper layer, consistent with Benjamin's[5] proposal for gravity currents. They found the bore speed is given by

$$\frac{u_{br2}^2}{g_2' d_2'} = \frac{(2H_2 - d_2' - d_2)(H_2 - d_2')d_2'}{H_2(H_2 d_2' + H_2 d_2 + d_2'^2 - 3d_2' d_2)}. \tag{5}$$

This expression reduces to (1) in the limit $d_2 \to 0$ (so that $d_2' \to \Delta d_2$). The expression also reduces to the linear long-wave speed in the limit $d_2' \to d_2$.

Using symmetry, as in the derivation of (2), the speed of an intrusion in a three-layer fluid is found by extending the result (5). Setting $H_2 = H/2$ and $d_2 = d/2$ in (5) gives

$$\frac{u_{br3}^2}{g\sigma(d+\Delta d)} = \frac{(2H-2d-\Delta d)(H-d-\Delta d)(d+\Delta d)}{4H[H(2d+\Delta d)-(d+\Delta d)(2d-\Delta d)]}. \tag{6}$$

In the limit of an infinitely deep fluid ($H \to \infty$), the bore speed becomes

$$C_{br} = \sqrt{\frac{g\sigma}{2}\frac{(d+\Delta d)^2}{2d+\Delta d}}. \tag{7}$$

This reduces to (4) in the limit $d \to 0$.

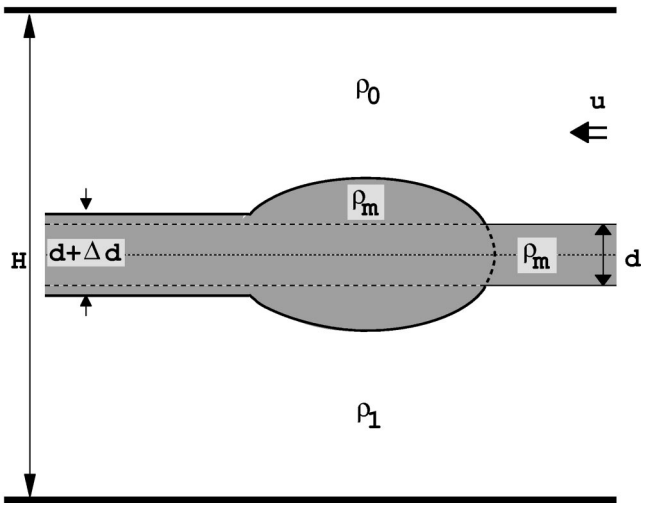

FIG. 2. Schematic of an intrusive gravity current in a three-layer fluid. The density of the intrusion is the same as the density of the middle layer.

Figure 3 shows the predicted bore speeds in two- and three-layer fluids. The speeds are given relative to the two-layer intrusion speed, C_{gc}. The plots show that, although there may be some uncertainty in the measurement of Δd, there is relatively small uncertainty in C_{br}. The relative speed of the bore is smaller in finite-depth fluid, but the difference is less than 10% for typical experimental values.

In all the theories presented above, it is assumed the bore or gravity current is steadily supplied with fluid so that it propagates in quasi-steady state. In the lock-release experiments of bottom-propagating gravity currents, this assumption is valid until the gravity current propagates a distance between 6 to 10 lock-lengths from the lock. After traveling this distance, an inverted bore (produced by the reflection of the return flow in the lock) catches up with the gravity current and slows its progress.[32] However, as illustrated in Fig. 4, such deceleration is not observed for intrusions. The diagrams show the results of three experiments, one of a gravity current propagating along the bottom of the tank in a one-layer fluid, one of an intrusion propagating along the interface of a two-layer fluid, and one of an intrusion into the middle layer of a three-layer fluid. In the first case, salt and dye are added to the fluid in the lock so that the relative density difference between the lock fluid and the ambient is $\sigma=0.019$. In the second case, the relative density difference between the upper and lower layers is $\sigma=0.028$ and the fluid in the lock is mixed so that its density is the average of the upper and lower layer fluids. In the third case the relative density difference between the upper and lower layers is $\sigma=0.018$ and the middle layer, which is 3 cm thick, has the same density as the fluid in the lock. The lock length is the same ($\ell=8.4$ cm) in all three experiments.

Horizontal time series are used to determine the position of the front of the gravity current and intrusion over time. The front position is plotted to the right in Fig. 4. Nondimensional times t/T are plotted in which the time-scale $T=\ell(g\sigma H)^{1/2}$ and H is the total depth of the ambient fluid. While the bottom-propagating gravity current clearly decelerates after it propagates approximately 100 cm from the lock, the intrusions maintain an almost constant speed over the same time and distance traveled. However, the intrusion in the three-layer fluid stops propagating midway along the tank and a double-humped solitary wave continues to propagate to the end of the tank.

In summary, although the behavior of the intrusion is examined in detail between 6 and 10 lock lengths from the lock-end of the tank, the dynamics of the rear bore interacting with the intrusion head are not expected to play a significant role in what is observed.

B. Internal waves

The characteristics of the observed internal waves may be compared with those derived for a three-layer fluid of total depth H and middle-layer depth d. Analytic solutions may be found if the thicknesses of the upper and lower interfaces are assumed to be zero and the system is assumed to

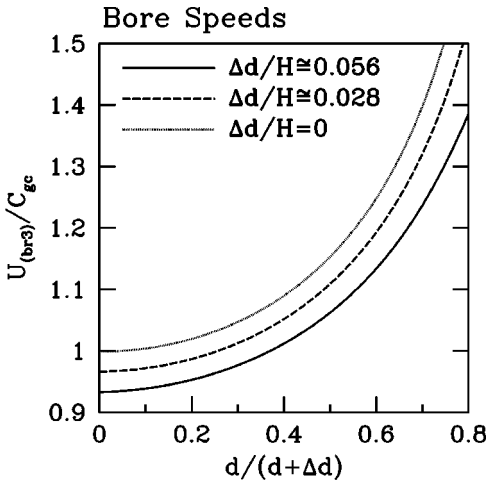

FIG. 3. Normalized speed of an intrusion in a three-layer fluid as a function of the relative change in the middle-layer depth, $d/(d+\Delta d)$. Values are shown for a fluid of depth $H=18$ cm and $\Delta d=1.0$ cm (solid line); $H=18$ cm and $\Delta d=0.5$ cm (dashed line); and $H\to\infty$ and $\Delta d=1.0$ cm (dotted line). The bore speed is normalized by the predicted speed, C_{gc}, of a gravity current in an infinitely deep two-layer fluid.

be spanwise uniform and of infinite horizontal and vertical extent. The ambient stepwise-continuous density profile is given by

$$\rho^{\text{step}}(z)=\begin{cases}\rho_0, & d/2<z<H/2,\\ \rho_m, & -d/2\leqslant z\leqslant d/2,\\ \rho_1, & -H/2<z<-d/2.\end{cases} \tag{8}$$

(Here, for mathematical convenience, $z=0$ corresponds to the fluid's mid-depth.) The displacement from equilibrium of the upper and lower interfaces is η_1 and η_2, respectively. These are assumed to be small compared with the wavelength of the disturbances, so that linear theory can be applied. Wavelike solutions are assumed so that $\eta_j(x,t)=A_j e^{i(kx-\omega t)}$ for $j=1,2$.

Assuming the flow in each layer is inviscid, irrotational, incompressible, and not diffusive, the motion in each layer can be described by velocity potentials ϕ_0, ϕ_1, and ϕ_2 for the upper, middle, and lower layers, respectively. The boundary conditions require continuity and zero stress across the interfaces and vanishing vertical velocities at the upper and lower boundaries of the domain. The resulting boundary value problem has been well studied in general.[33,34] The resulting set of equations form an eigenvalue problem in which the eigenvalue is the dispersion relation $\omega=\omega(k)$ and the corresponding eigenfunction gives the structure of the wave modes.

With the assistance of the symbolic algebra program, Maple, the analytic form of the dispersion relation is found. In the simple case of an infinitely large domain, the dispersion relation is given implicitly by

$$(\omega^2)^2\left[1-\frac{\sigma^2(1-\gamma)}{16}\right]-(\omega^2)\left[\frac{1}{2}g\sigma k\right]+\left[\frac{1-\gamma}{16}(g\sigma k)^2\right]=0, \tag{9}$$

where $\gamma=\exp(-2kd)$. The two roots of the quadratic equation for ω^2 correspond to the dispersion relations for the

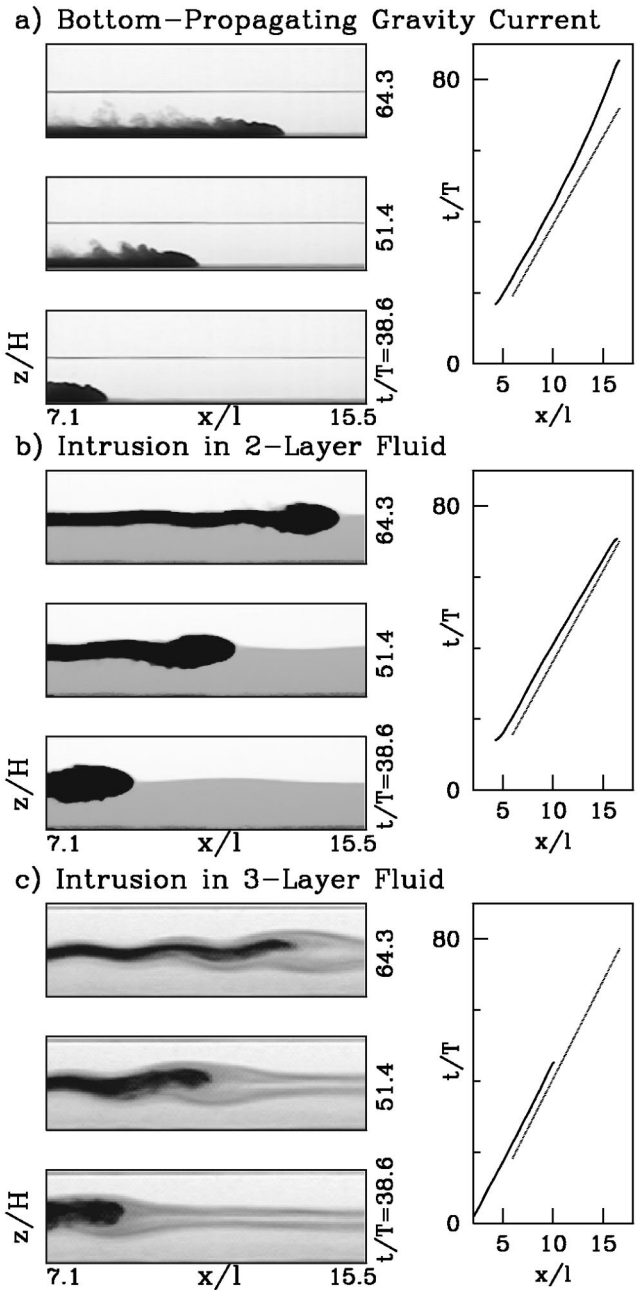

FIG. 4. Propagation of (a) a gravity current along the bottom of a tank in a one-layer fluid of depth 8.5 cm, (b) an intrusion along the interface in a two-layer fluid, each layer of depth 8.5 cm (the bottom layer appears gray), and (c) an intrusion into the middle layer of a three-layer fluid (the upper and lower interfaces appear light gray). In all three cases the fluid from the lock is dyed so that it appears black in the images. The images to the left show the nondimensional position (x/ℓ) and structure of the gravity current/intrusions at nondimensional times $t/T=38.6$, 51.4, and 64.3 s after the gate is extracted. The plots to the right show the position over time (solid line) of the front of the gravity current/intrusion. The dotted line is the offset best-fit line to the data between $x/\ell=4.8$ and 9.6. Notice the deceleration of the bottom propagating current at late times. Also note that the intrusion in three-layer fluid stops propagating after approximately ten lock-lengths.

even (sinuous) and odd (varicose) modes. It can be shown that both roots are positive so there are no unstable modes of the system (ω is real). The corresponding eigenfunctions reveal the structure of the modes. For the even (odd) modes, A_1 and A_2 are of the same (opposite) sign. For fixed k, the frequency of the even mode is larger than that of the odd mode. In the long wavelength limit $kd\to 0$, the dispersion relation of the even mode is the same as that for internal waves in a two-layer fluid. In particular the phase speed, $c_p=\omega/k$, of the even and odd modes are

$$C_e=\sqrt{g\sigma/2k} \tag{10}$$

and

$$C_o=\sqrt{g\sigma d/2}, \tag{11}$$

respectively. The phase speed of the odd mode is typically much smaller than that of the even mode if the depth, d, of the middle layer is relatively small compared with the horizontal wavelength $\lambda=2\pi/k$.

The relationship between the predicted phase speed and wavenumber is shown in Fig. 5 for (a) even and (b) odd modes with $\sigma=0.02$ and $d=2$ cm. In each diagram the phase speed relationship is shown for an infinitely deep fluid (dashed-line) and a fluid with $H=18$ cm (dotted-line). The horizontal axis is the nondimensional wavenumber kd and the phase speed is normalized by C_{gc}, given by (4).

For $kd\gtrsim 0.4$ the phase speed relation between the infinite-depth and finite-depth fluids is approximately the same. Finite-depth effects are most pronounced for the even modes with $kd\ll 0.4$. In a finite-depth fluid the phase speed approaches a constant value (dependent upon H) as the wavenumber becomes small, whereas the phase speed is unbounded in an infinitely deep fluid.

Benjamin[5] showed that waves should not occur in the lee of a bottom-propagating gravity current. Effectively this is because the phase speed of shallow water waves, which depends on the depth of the tail of the current, is slower than the gravity current speed: the waves are supercritical. The analogous waves in a three-layer fluid are odd-mode disturbances, which Fig. 5 shows are indeed supercritical. However, the phase speed of long wavelength even modes is dependent not upon the depth d of the interface, as in (11). Rather, it depends upon the wavenumber k, as in (10): the long wave even modes have faster phase speed. Indeed, in the experiments reported here, the waves are subcritical. It is fundamentally for this reason that waves are excited in the lee of an intrusion, though not in the lee of a bottom-propagating gravity current.

Using a numerical code that solves the Taylor–Goldstein equation,[34,35] the dispersion relation of these modes can be determined in a fluid where the upper and lower interfaces of the middle layer have finite thickness $D>0$. Rather than a discontinuous jump in density across each interface, the density profile is assumed to vary as a hyperbolic tangent function. This variation has been shown to approximate closely the accurately measured density profile in a series of lock-release experiments.[27]

The phase speed relation for the even and odd modes is plotted as the solid line in Fig. 5 for the case with $D=0.5$ cm. There is negligible difference between this line and that calculated for the even mode of a three-layer fluid with $D=0$. Thus the thickening due to mixing of the upper and lower interfaces of the middle layer does not significantly affect the characteristics of sinuous waves. For the

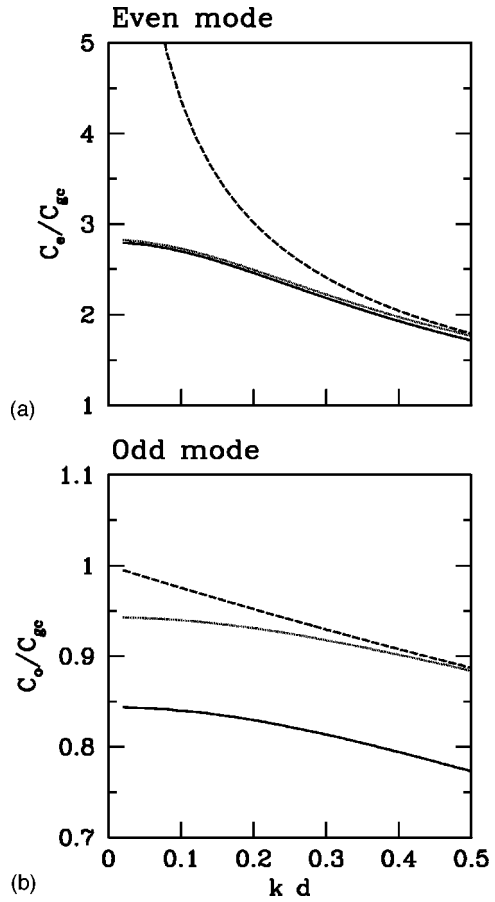

FIG. 5. Normalized phase speeds versus normalized wavenumber for (a) even mode and (b) odd mode internal waves in a three-layer fluid with $\sigma = \Delta\rho/\rho_m = 0.02$ and $d = 2$ cm. The dispersion relationships are calculated for a fluid with interface thickness $D = 0.5$ cm and total depth $H = 18$ cm (solid line), $D = 0$ and $H = 18$ cm (dotted line), $D = 0$ and $H \to \infty$ (dashed line). The phase speeds are normalized by the gravity current speed c_{gc} given by (4), with $\Delta d = 1.0$.

even modes, the effects of the interface thickness should become important for waves with wavenumber $k \gtrsim 1/D$.

Even if k is small, the phase speed of the odd modes is reduced if the interfaces are thick. The degree to which it is reduced is found to be a function of the interface thickness D. This is anticipated because the middle layer is alternately compressed and stretched due to the motion of long-wavelength varicose waves and the motion therefore should depend sensitively upon the structure of the middle layer.

In experiments, the wave train behind the head of the intrusion is observed to have the structure of even modes with moderately small wavenumbers. The theory presented here shows that their dynamics are well represented by an analytic model in which the background density profile is stepwise-continuous.

C. Solitary waves

A large-amplitude disturbance on relatively shallow water may develop to form a coherent structure in the form of a solitary wave. Solitary waves in a two-layer fluid have been studied theoretically in considerable detail.[12–16,20,36,37] Typically, an internal solitary wave is an elevated hump if the depth of the upper layer is greater than the depth of the lower layer. It is a wave of depression if the depth of the upper fluid is less than that of the lower fluid.

Extending these concepts to a symmetric three-layer fluid, in which the upper and lower layer depths are equal, a solitary wave may develop in the form of a double-humped wave propagating along the middle layer [see Fig. 1(c)]. The middle layer thus plays the role of a shallow fluid that both underlies the deeper upper layer (and so a hump of elevation may exist at the upper interface) and overlies the deeper lower layer (and so a hump of depression may exist at the lower interface). The experiments show that the two disturbances are phase-locked propagating as a single disturbance with the symmetry of odd (varicose) internal wave modes.

In view of the above analyses of internal wave dispersion relations, the speed of the observed double-humped solitary wave is expected to be overpredicted in a theory that does not account for the effects of thick upper and lower interfaces. A rigorous derivation of the solitary wave speed in a fluid with thick interfaces is beyond the scope of this work. Rather, an estimate of the solitary wave speed in a stepwise-continuous three-layer fluid is determined by extending well-known theories of internal solitary waves in a two-fluid system.

The theoretical study of internal solitary waves was initiated by Keulegan[12] who extended the work of Korteweg and deVries[38] (KdV) to a Boussinesq two-layer fluid with a free surface. In the development of the resulting ''KdV'' equation, it is assumed that the amplitude A_{sw} is related to the horizontal extent, λ, of the waves by the scaling

$$A_{sw}/d_2 = O\left(\frac{d_2^2}{\lambda^2}\right), \tag{12}$$

where d_2 is the depth of the (shallow) bottom layer. For relatively small-amplitude waves ($A_{sw}/H_2 < 0.05$), experiments have shown that under the scaling (12) the KdV equation is a good description of the speed and structure of waves.[17,20]

In the experiments reported here, the analogous amplitude of the observed solitary wave is larger than 0.05, the half depth of the fluid, and so a KdV theory is not well adapted for comparison with the experimental results. In this case the return flow of the ambient fluid is sufficiently large that the structure and speed of the solitary wave are modified. A more accurate representation of the solitary wave dynamics is given by adapting the large-amplitude solitary wave theory that combines results of a KdV and ''modified-KdV'' theory.[39–41] With rigid upper and lower boundary conditions and for a Boussinesq fluid, the large-amplitude KdV theory predicts the speed of a large-amplitude internal solitary wave to be[19]

$$u_{sw2} = \sqrt{g_2' H_2/4}\left[1 - \frac{2}{H_2^2}(A_{sw} - \overline{h})^2\right], \tag{13}$$

in which $\overline{h} \simeq H_2/2 - d_2$, and we have assumed $\rho_m/\rho_0 \simeq 1$. The structure of the wave is given by

$$\eta = A_{sw} \frac{\mathrm{sech}^2[\kappa(x-u_{sw2}t)]}{1-\mu \tanh^2[\kappa(x-u_{sw2}t)]}, \tag{14}$$

where $\kappa \simeq [12A_{sw}(2\overline{h}-A_{sw})]^{(1/2)}/H_2^2$ and $\mu \simeq (2\overline{h}-A_{sw})/A_{sw}$. Note that if $A_{sw}=\overline{h}$, (14) becomes $\eta = A_{sw}$, a constant. The distance between the interface and the two-layer fluid's mid-depth, $\overline{h}$, is the limiting amplitude of the solitary wave. The use of modified KdV theory is appropriate only if the wave amplitude is close to this limiting amplitude. In Sec. IV C we show this is indeed the case.

As above, the symmetry of the double-humped solitary waves is exploited to derive a simple extension of KdV theory. Assuming the streamline at mid-depth in the fluid is horizontal, we let $H=2H_2$ and $d=2d_2$ in (13) to find the solitary wave speed

$$u_{sw3} = \sqrt{\left(\frac{g\sigma H}{16}\right)}\left[1-8\frac{(A_{sw}+H/4-d/2)^2}{H^2}\right], \tag{15}$$

where A_{sw} is the maximum vertical displacement of the upper interface.

The KdV theory has been modified to account for larger amplitude effects.[37,39–41] Two-layer internal solitary wave theory has been generalized to non-Boussinesq fluids[13] and to fluids with infinitely large upper layer depth.[13,15,16] However, the required scaling of these theories lies beyond the regime for the waves observed in the experiments reported upon here.

D. Momentum budget

In order to assess the relative dynamical importance of the trailing internal waves and the solitary waves to the evolution of the intrusion, the momentum flux associated with each is estimated.

For $d \ll H$ the mass per unit width of the intrusion is approximately $\rho_m \ell H$. Given the initial velocity c_i, the total momentum of the initial intrusion is approximately

$$M_i = \rho_m \ell H c_i. \tag{16}$$

At a distance L_{sw} from the lock, the intrusion stops propagating and its momentum is lost to the internal waves and the solitary wave. To estimate the momentum extracted from the intrusion, imagine a control volume which surrounds the head of the intrusion and which is stationary in a reference frame moving with speed c_i. The divergence of the momentum flux, $\mathcal{F}=\int \rho_m |\underline{u}|^2\, dz$, integrated over the control volume gives the momentum extracted per unit time from the intrusion. Based on experimental observation, we assume internal waves are continuously excited by the intrusion until it stops propagating and the solitary wave is generated. The time over which this occurs is approximately L_{sw}/C_i. The velocity field, $\underline{u}$, of internal waves is estimated using the stepwise-continuous three-layer model described in Sec. III B. In the limit of internal waves that are long with respect to the middle-layer depth and are short with respect to the total fluid depth,

$$M_{iw} \approx L_{sw}\rho_m A_{iw}^2 \frac{g\sigma}{2}/c_i, \tag{17}$$

where A_{iw} is the maximum vertical displacement of the waves. In particular, (17) shows that M_{iw} should be proportional to the square of the wave amplitude, A_{iw}.

The momentum extracted by the solitary wave is estimated to be twice the momentum extracted by the modified KdV solitary wave in a two-layer fluid: $2\int(\int_0^\eta \rho_m u\, dz)\, dx$, where η is the displacement of the upper interface given by (14). Using equations for incompressible fluid,

$$M_{sw} = 2\rho_m c_{sw}\int_{-\infty}^{\infty} \eta\, dx \simeq 2\rho_m c_{sw}\left(\frac{2A_{sw}Hd^2}{3}\right)^{1/2}, \tag{18}$$

where c_{sw} is the speed of the solitary wave.

IV. ANALYSIS OF EXPERIMENTS

In this section, the observed properties of the interfacial gravity current and the waves it generates are presented and compared with theory. The focus of these analyses is to understand the transition in the dynamics of an intrusion as it propagates into a three-layer fluid with a middle layer of different widths.

A. Intrusive gravity current

Horizontal time series of digitized images of the experiments are used to estimate the speed of the intrusive gravity current and the phase speed and wavelength of trailing internal waves. For example, Fig. 6 shows the horizontal time series taken from a cross section along the length of the tank during an experiment in which an intrusion propagates into a two-layer fluid with $\sigma=0.033$. Time $t=0$ corresponds to the moment when the lock is released. The slope of the lowest dark band gives the horizontal speed of the intrusion. The slope of the bands at later times give the phase speed of successive trailing internal waves. This image shows three trailing waves behind the intrusion. In horizontal time series taken from experiments in which an intrusion propagates into a three-layer fluid, the trailing internal waves form a quasi-monochromatic wave train and the phase speed of the waves is moderately faster than the speed of the intrusion itself.

The second column of Table I lists the measured speeds of intrusions propagating along the interface of a two-layer fluid. The third column compares the results with the predicted gravity current speed given by (4), in which we have used the estimate $\Delta d = \epsilon H \simeq 0.8$ cm. In each case, we find the observed speed is larger than C_{gc} by approximately 50%. The discrepancy is attributed to overestimation of Δd: the depth of the tail behind the gravity current head is in fact smaller than the ultimate thickening of the middle layer. Though the relative discrepancy is independent of σ, it changes with the lock length. In experiments with locks five times longer, we find the ratio of the observed speed to C_{gc} is approximately equal to 1.

Figure 7 plots the observed speed, c_i^{obs}, of an intrusion moving horizontally into a three-layer fluid for a range of experiments with different middle-layer depths, d, and relative density differences, σ. In all experiments $\ell = 8.4$ cm. Hence, $\epsilon H = (\ell/L)H \simeq 0.8$ cm. The normalized speed is rep-

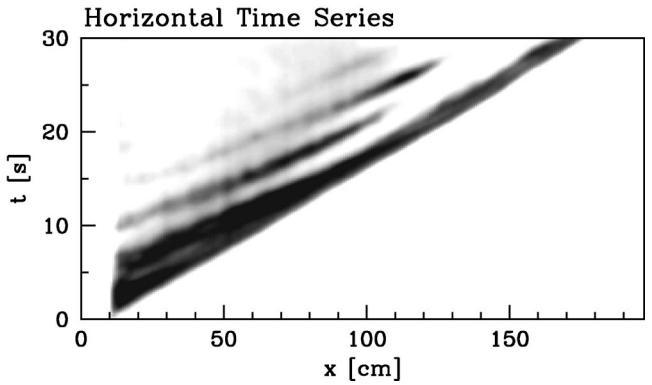

FIG. 6. Horizontal time series taken from experiments showing the motion of the intrusion and trailing internal waves 0.5 cm below mid-depth over the entire length of the tank. The time series is shown over 30 s after the lock (with $\ell = 8.4$ cm) is released.

resented by a Froude number $\mathrm{Fr}_i = c_i^{\mathrm{obs}}/[g\sigma(d+\epsilon H)/2]^{(1/2)}$. If the depth of the tail behind the intrusion, Δd, was equal to the anticipated ultimate thickening of the middle layer ϵH, then (7) predicts $\mathrm{Fr}_i \simeq 1/2^{(1/2)}$, in the limit $H \to \infty$ and $\Delta d \ll d$. However, when plotted against $\epsilon H/(d+\epsilon H)$, the experimental data collapse approximately onto a straight line passing through the origin. The slope of the best fit line through the points and the origin is 3.10 ± 0.02.

These observations allow us to predict that, if $\epsilon H \ll d$, the speed of the intrusion depends upon d and σ according to

$$c_i \propto \epsilon H (g\sigma/d)^{(1/2)}. \tag{19}$$

This result is contrary to (7), which predicts that the intrusion speed should be an increasing function of d. However, the theory assumed that the bore is supplied with an infinite volume of fluid, whereas the experiments supply a finite volume of fluid, characterized by the value of ϵH. Thus, unlike two-layer fluid experiments, the lock length is a non-negligible parameter in determining intrusion speeds.

Measurements of intrusion speeds in a three-layer fluid are listed in the fourth column of Table I. The intrusion speeds are consistently slower than those of intrusions in a two-layer fluid. The fifth and six columns of Table I show that the phase speeds of trailing internal waves and of the leading solitary wave are moderately faster than the intrusion. This is discussed further in the sections below.

TABLE I. Gravity current speeds, c_{gc}, along an interface in two-layer experiments, intrusion speeds, c_i, in three-layer experiments, and corresponding relative internal wave speeds and solitary wave speeds.

	$d=0$ cm		$d \simeq 3.7$ cm		
σ	c_{gc} (cm/s)	$c_{\mathrm{gc}}/C_{\mathrm{gc}}$	c_i (cm/s)	c_{iw}/c_i	c_{sw}/c_i
0.002	1.4	1.6	1.2	1.3	1.2
0.007	2.9	1.7	2.3	1.2	1.2
0.017	4.0	1.5	1.3	1.2	1.1
0.033	5.5	1.5	4.7	1.1	1.1

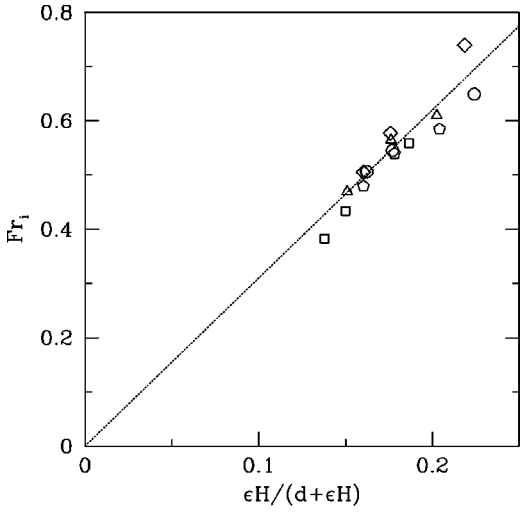

FIG. 7. Values of $\mathrm{Fr}_i = c_i^{\mathrm{obs}}/[g\sigma(d+\epsilon H)/2]^{(1/2)}$ plotted against $\epsilon H/(d+\epsilon H)$ for five experiments of an intrusion into a three-layer fluid with $\sigma = 0.002$ (triangles), 0.004 (squares), 0.007 (diamonds), 0.017 (pentagons), and 0.033 (circles). For each experiment, three runs are performed with d ranging from 3 to 5. In each case, $\epsilon H \simeq 0.8$ cm is constant. The diagonal dashed line is the best fit line through the data and the origin.

B. Internal waves

Though internal waves are always observed behind the gravity current, their number and amplitude are large if the width, d, of the middle interface is large. The resonant excitation of internal waves is clearly demonstrated in Fig. 8 which shows time series of a vertical cross section of the tank during the passage of a successive series of intrusions. The middle layer and intrusions are dyed with different colors so that their motions may be visualized.

In run 1 (top) the intrusion passes along the interface of a two-layer fluid. The time series is shown for 38 s, shortly before the head of the intrusion arrives at the position of the vertical cross-section (about 80 cm from the lock-end of the tank). The time series clearly shows sinusoidal oscillatory motion due to even-mode internal waves trailing behind the intrusion. The waves persist for approximately three periods.

As a result of interfacial mixing by the intrusion, the middle interface broadens. In run 2, the experiment is repeated by releasing an intrusion into this approximately three-layer fluid. The vertical time series shows that waves are excited over longer times after the intrusion has passed. In successive runs, as the depth of the middle layer increases, larger amplitude waves are excited for longer times. The average amplitude is found by measuring half the vertical distance between adjacent crests and troughs in the time series.

The frequency of the waves may be determined from images of the vertical times series, as shown in Fig. 8, and from horizontal time series, such as that shown in Fig. 6.

Horizontal time series are also used to measure the wavelength, λ, of the trailing internal waves. In experiments with a range of σ and d, we find typically $\lambda = 20(\pm 1)$ cm. The corresponding wavenumber is $k = 0.31(\pm 0.01)$ cm^{-1}. The wavelength is a weak function of the lock length, increasing by 10% as the lock length increases fivefold. In experiments in fluids with double the total depth, H, we find

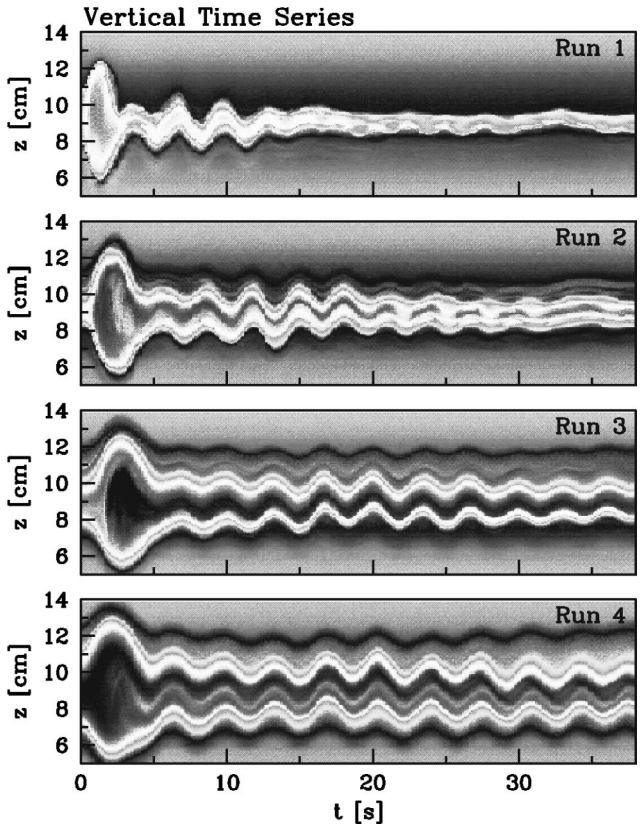

FIG. 8. False-color vertical time series taken for successive runs in an experiment. The middle layer is dyed to visualize the vertical motion of the intrusion and trailing internal waves.

the wavelength also doubles so that kH remains approximately constant. The wavelength is set by the scale of the gravity current head, which has comparable horizontal extent.

The particular internal wave mode excited (even or odd, in a three-layer theory) is determined by the excitation frequency of the waves. In all experiments, the excitation frequency is sufficiently large that even-mode waves are always observed. The excitation frequency is set by the speed of propagation of the intrusion. Indeed, experiments show that the phase speed of the waves is comparable, though slightly faster than the speed of the intrusion.

Figure 9 compares the observed phase speed with that predicted by an approximate linear theory. The plot shows values of the internal wave Froude number, $\mathrm{Fr}_{\mathrm{iw}}=c_p^{\mathrm{obs}}/C_e$, versus the nondimensional wavenumber, kH, which a range of experiments show is approximately constant for a wide range of values of ℓ, d, σ, and H. We normalize by C_e because $kd>0.8$ in all the experiments and therefore the predicted phase speed in infinite fluid is approximately equal to that in finite depth fluid with $H=18$ cm. Typically the discrepancy is less than 0.5%. Generally the wavelength is moderately larger than the total depth of fluid in the tank. Likewise, we find that the Froude number lies within the narrow range $0.7\lesssim \mathrm{Fr}_{\mathrm{iw}}\lesssim 0.9$. Thus the phase speed of the even-mode internal waves is consistently overpredicted by (10).

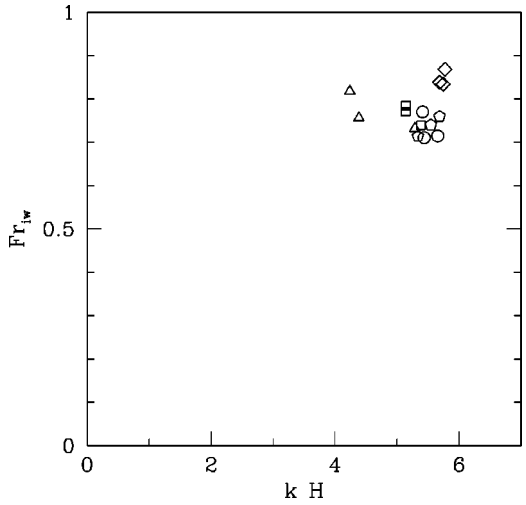

FIG. 9. Values of the $\mathrm{Fr}_{\mathrm{iw}}=c_p/C_e$ plotted against kH for five experiments of an intrusion into a three-layer fluid with $\sigma=0.002$ (triangles), 0.004 (squares), 0.007 (diamonds), 0.017 (pentagons), and 0.033 (circles). For each experiment, three runs are performed with d ranging from 3 to 5. In each case, $\epsilon H\simeq 0.8$ cm is constant.

The second to last column in Table I shows that the speed of the internal waves is typically faster than the speed of the intrusion. Thus, consistent with Fig. 5, even-mode instead of odd-mode internal waves are generated behind the intrusion.

The efficiency with which the intrusion excites internal waves is evaluated by measuring the amplitude of the waves. Table II lists measured amplitudes of the waves in experiments with middle interface widths of $d=3$ and 4 cm and different relative density differences, σ. The table shows that the amplitude of the waves decreases as σ increases, but the amplitude is relatively insensitive to the value of d over the range investigated. The wave amplitudes are approximately 2% of their horizontal wavelength. In comparison, the maximum amplitude of deep water waves before breaking is 7% of their horizontal wavelength.[42] Thus, although 2% is a small number, it appears to be sufficiently large that the wave speed is adjusted by nonlinear effects. This may explain the discrepancies between linear theory and the observations in Fig. 9.

C. Solitary wave

If the middle layer is sufficiently wide, the intrusion is observed to stop propagating and a double-humped solitary wave is generated. The solid curves in Fig. 10 show the observed displacement of the upper interface due to the passage of the solitary wave in experiments with $d=3$ and 4 cm. In both experiments the three-layer fluid is set up initially with thin dye lines marking the positions of the upper and lower interfaces. For both, $\sigma=0.027$ and $\epsilon H\simeq 0.8$. The structure of the upper interface is reconstructed from a vertical time series of the experiment taken 150 cm from the lock-end of the tank. Specifically, a contour is matched to the edge of the upper dye line and its vertical position as a function of time $\eta(t)$ is recorded. Observing that the motion of the solitary wave is close to steady state, moving with speed

TABLE II. Observations of internal wave amplitudes (A_{iw}), propagation distance of intrusion (L_{sw}), and estimates of the initial momentum flux per unit mass associated with the intrusion M_i/ρ_m. Also given is the the relative momentum extracted by internal waves M_{iw}/M_i and by solitary waves M_{sw}/M_i. Values of A_{iw} and L_{sw} are given in centimeters and of M_i/ρ_m in cm^3/s. Upper bounds on the errors are estimated to be $\pm 5\%$ for M_i, $\pm 20\%$ for M_{sw}, and $\pm 25\%$ for M_{iw}.

	$d=3$ cm				
σ	A_{iw}	L_{sw}	$\frac{M_i}{\rho_m}$	$\frac{M_{iw}}{M_i}$	$\frac{M_{sw}}{M_i}$
0.0025	0.44	110	1.5×10^2	0.17	0.74
0.01	0.39	90	3.0×10^2	0.11	0.74
0.02	0.37	140	4.2×10^2	0.16	0.74
0.03	0.34	180	5.2×10^2	0.17	0.74
		$d=4$ cm			
0.0025	0.45	80	1.5×10^2	0.13	0.91
0.005	0.42	95	2.1×10^2	0.14	0.91
0.01	0.41	97	3.0×10^2	0.13	0.90
0.02	0.32	97	4.2×10^2	0.08	0.91
0.03	0.36	110	5.2×10^2	0.12	0.90
0.04	0.32	112	6.0×10^2	0.10	0.90
0.05	0.19	120	6.7×10^2	0.04	0.90

c_{sw}, the spatial structure of the interface is given by $\eta(x) \equiv \eta(-c_{sw}t)$. The plot is then shifted in x so that the position of the the maximum occurs at $x=0$ and it is shifted in η so that the mean value between to the crest and trough of the trailing internal wave (to the left of the solitary wave) corresponds to $\eta=0$.

The plots demonstrate the difficulty in defining solitary wave amplitudes: the distance from the peak of the solitary wave to initial level of the interface (to the right of the wave) is greater than the distance to the mean level of the trailing internal waves. The difference can be as large as 1 cm. We have chosen to define the amplitude with respect to the level of the interface trailing the waves because theory then gives the closest agreement with observations.

In experiments with a wide range of σ, the amplitudes are typically $A_{sw} \simeq 2.0$ in experiments with $d=3$ cm, and A_{sw} is 10% smaller in experiments with $d=4$ cm. In all cases the $A_{sw}+d/2$ is only moderately less than the critical amplitude $A_c \simeq H/4$. This justifies our use of the modified KdV theory[40,41] for analyzing the waves.

The predicted structure of an internal solitary wave in a two-layer fluid is superimposed on the plots in Fig. 10. The dashed line shows the amplitude predicted by modified KdV theory, (14). Though the agreement is good near the peak of the waves, the predicted width is wider than observed. In comparison, the width of classical KdV solitons (not shown) is less than half that of the observed width.

The modified KdV theory does a poor job predicting the wave speed. The predicted speed, given by (15), is typically three to four times larger than the observed speed. In part this may be attributed to the non zero thickness of the upper and lower layer fluid interfaces and also due to interactions with trailing internal waves.

In our analyses, we find the solitary wave speed compares better with C_o as given by (11). Figure 11 shows the observed solitary wave speeds in experiments with a range of values of d and σ, and with $\epsilon H=0.8$ cm fixed. The normalized speeds are represented by a Froude number $\mathrm{Fr}_{sw} = c_{sw}^{obs}/[g\sigma(d+\epsilon H)/2]^{(1/2)}$. As with the intrusion speeds, we find that Fr_{sw} varies linearly with $\epsilon H/(d+\epsilon H)$ over the range of data shown. The best fit line through the data points and the origin has slope 3.51 ± 0.04. The slope is 13% larger than that determined for the intrusion. This is consistent with the data in the last column of Table I, which shows the solitary wave speed is 10%–20% faster than the intrusion speed.

We have not been able to assess the dependence of the solitary wave speed upon amplitude because only a limited range of amplitudes are generated by the method we employ to create the waves.

Table II lists the observed maximum horizontal distance, L_{sw}, to which the fluid originating from the lock propagates and beyond which a solitary wave travels. The values are accurate to within 2 cm. For fixed σ, the solitary wave appears at a further distance L_{sw} along in the tank when $d=3$ cm than it does when $d=4$ cm. If d is fixed, the solitary wave appears further along in the tank for a higher σ.

In a series of experiments in which a three-layer system is created by repeatedly releasing an intrusion into a two-layer system, the effect of changing the lock-length ℓ is observed. For a fixed value of σ, the distance d at which the solitary wave is excited is measured on the third run of three

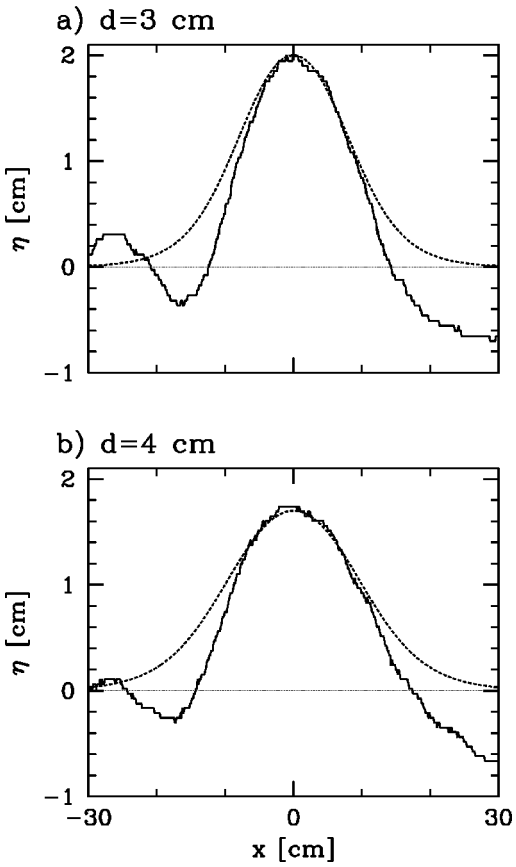

FIG. 10. Comparison between the observed displacement of the upper interface by a solitary wave (solid line) and that predicted by modified-KdV theory (dashed line). Results are shown for two experiments in which the middle interface thickness is (a) $d=3$ cm and (b) $d=4$ cm.

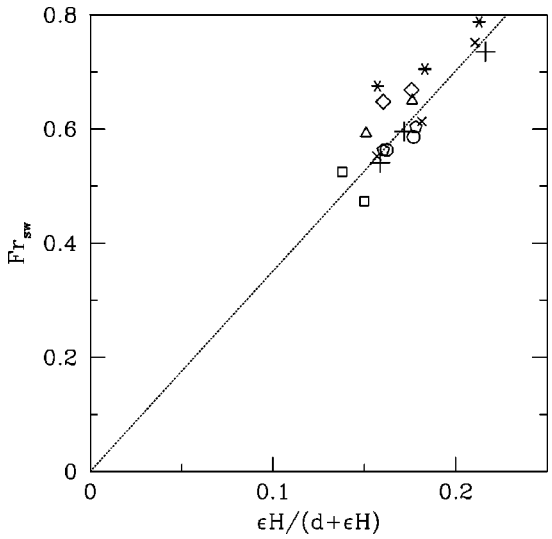

FIG. 11. Values of $\mathrm{Fr}_{\mathrm{sw}}=c_{\mathrm{sw}}^{\mathrm{obs}}/[g\sigma(d+\epsilon H)/2]^{(1/2)}$ versus $\epsilon H/(d+\epsilon H)$ in two runs each of five experiments with $\sigma=0.002$ (triangles), 0.004 (squares), 0.007 (diamonds), 0.017 (pentagons), and 0.033 (circles), and in three runs each of three experiments that are set up initially as three-layer fluids with $\sigma=0.004$ (upright cross), $\sigma=0.008$ (diagonal cross), and $\sigma=0.014$ (star). The diagonal dashed line is the best fit line through the data and the origin.

different experiments with $\ell=20$, 30, and 40 cm. As expected, intrusions released from longer locks result in a larger increase in interfacial layer thickness, which in turn corresponds to smaller L_{sw}. The factors governing the value of L_{sw} are examined below.

D. Momentum balance

By experimentally determining the amplitude and frequency of the waves, the momentum of the intrusion, M_i, and the amount extracted by the internal waves, M_{iw}, and the solitary wave, M_{sw}, can each be determined. These values are listed in Table II.

Upper bounds on the error are estimated to be $\pm 5\%$ for M_i, $\pm 20\%$ for M_{sw} and $\pm 25\%$ for M_{iw}. The large source of error for the computed internal and solitary wave momentum flux lies in the sensitivity to the data. For the internal wave momentum flux, there is a strong dependence on the accuracy of the wave amplitude.

The table shows that the momentum of the intrusion increases with increasing σ. This is expected because the intrusion propagates faster if the vertical density gradient is larger. The table also shows that the momentum extracted by the internal and solitary waves increases with increasing σ so that the sum is approximately equal to M_i.

Despite the crudeness of the approximations, it is surprising to find how well the estimates predict a balanced partition of extracted momentum by internal and solitary waves. For fixed d, an approximately constant fraction of the intrusion's momentum is extracted by the solitary wave. This occurs because the wave has a fixed size and speed which depends on the initial setup of the experiment. The momentum extracted by the internal waves M_{iw}, which makes up the difference, is less than one-fifth the momentum of the intrusion, M_i. Since an increase in σ results in a greater initial momentum of the current, a greater amount of momentum must be transferred to the internal waves before a solitary wave can be excited. Consequently, the current must propagate further along the tank before momentum is completely lost to the trapped internal waves and the solitary wave.

Momentum balance can be used to predict the distance at which the solitary wave first appears. Supposing $M_i=M_{\mathrm{iw}}+M_{\mathrm{sw}}$, and rearranging the defining equations to isolate L_{sw} gives

$$L_{\mathrm{sw}}\simeq\epsilon^2\frac{H^3}{A_{\mathrm{iw}}^2}\times\left[1-\left(\frac{d}{\epsilon H}\right)^{3/2}\left(1+\frac{A_{\mathrm{sw}}}{d}\right)\left(\frac{8}{3}\frac{A_{\mathrm{sw}}}{H}\right)^{1/2}\right], \quad (20)$$

where the approximation $\Delta d\simeq\epsilon H$, has been used.

The distance L_{sw} traversed by the intrusion depends strongly on the depth d of the middle layer and on the amplitude A_{iw} of the trailing internal waves. As d increases, L_{sw} decreases. Because A_{iw} generally decreases with increasing σ, L_{sw} is an increasing function of σ.

V. CONCLUSIONS

We have shown that an intrusion in a three-layer fluid may excite both large-amplitude internal waves and solitary waves. The waves are continuously excited provided the middle layer is sufficiently wide. Two internal wave modes may be excited in theory, but only sinuous waves are observed in practice because their phase speed is close to the intrusion speed.

In comparison with idealized theories of two- and three-layer fluids, generally we find agreement to first order. Discrepancies are attributed to the relatively small volume of fluid in the intrusion and the non-negligible thickness of the interfaces between fluid layers of different density. Measurements of intrusion and wave speeds allow us to develop predictions based upon experimental parameters. In particular, when internal and solitary wave speeds are rescaled, experiments show the resulting Froude numbers exhibit linear dependence on $1/d$ if the lock length is sufficiently small.

The observed transition from two- to three-layer dynamics has important qualitative implications to the study of pollutant transport in stratified fluids. Though mass is transported a great distance along a thin interface, this is not the case if repeated mixing occurs or if the middle layer is sufficiently wide.

In the work presented here, the middle layer density is restricted to be equal to the mean of the upper and lower layer densities, and the depths of the upper and lower layers are the same. In a future study of a three-layer fluid, this restriction will be relaxed so that $\rho_1-\rho_0\neq\rho_2-\rho_1$.

ACKNOWLEDGMENTS

The experiments were performed in the Environmental and Industrial Fluid Dynamics Laboratory at the University of Alberta. This work has been supported by funding from the Natural Sciences and Engineering Research Council of Canada, 203065-99.

[1]J. E. Simpson, *Sea Breeze and Local Winds* (Cambridge University Press, Cambridge, England, 1994).
[2]P. F. Linden and J. E. Simpson, ''Microbursts: A hazard for aircraft,'' Nature (London) **317**, 601 (1985).
[3]J. E. Simpson, *Gravity Currents*, 2nd ed. (Cambridge University Press, Cambridge, England, 1997).
[4]G. H. Keulegan, ''An experimental study of the motion of saline water from locks into fresh water channels,'' Technical Report 5168 Nat. Bur. Stand. Rept. (1957).
[5]T. B. Benjamin, ''Gravity currents and related phenomena,'' J. Fluid Mech. **31**, 209 (1968).
[6]R. E. Britter and J. E. Simpson, ''Experiments on the dynamics of a gravity current head,'' J. Fluid Mech. **88**, 223 (1978).
[7]M. A. Hallworth, H. E. Huppert, J. C. Phillips, and R. S. J. Sparks, ''Entrainment into two-dimensional and axisymmetric turbulent gravity currents,'' J. Fluid Mech. **308**, 289 (1996).
[8]C. Härtel, L. Kleiser, M. Michaud, and C. F. Stein, ''A direct numerical simulation approach to the study of intrusion fronts,'' J. Eng. Math. **32**, 103 (1997).
[9]R. R. Long, ''Blocking effects in flow over obstacles,'' Tellus **22**, 471 (1970).
[10]I. R. Wood and J. E. Simpson, ''Jumps in layered miscible fluids,'' J. Fluid Mech. **140**, 329 (1984).
[11]J. B. Klemp, R. Rotunno, and W. C. Skamarock, ''On the propagation of internal bores,'' J. Fluid Mech. **331**, 81 (1997).
[12]G. H. Keulegan, ''Characteristics of internal solitary waves,'' J. Res. Natl. Bur. Stand. **51**, 133 (1953).
[13]T. B. Benjamin, ''Internal waves of finite amplitude and permanent form,'' J. Fluid Mech. **25**, 241 (1966).
[14]T. B. Benjamin, ''Internal waves of permanent form in fluids of great depth,'' J. Fluid Mech. **29**, 559 (1967).
[15]R. E. Davis and A. Acrivos, ''Solitary internal waves in deep water,'' J. Fluid Mech. **29**, 593 (1967).
[16]H. Ono, ''Algebraic solitary waves in stratified fluids,'' J. Phys. Soc. Jpn. **39**, 1082 (1975).
[17]C. G. Koop and G. Butler, ''An investigation of internal solitary waves in a two-fluid system,'' J. Fluid Mech. **112**, 225 (1981).
[18]A. P. Stamp and M. Jacka, ''Deep-water internal solitary waves,'' J. Fluid Mech. **305**, 347 (1995).
[19]H. Michallet and E. Barthélemy, ''Ultrasonic probes and data processing to study interfacial solitary waves,'' Exp. Fluids **22**, 380 (1997).
[20]H. Michallet and E. Barthélemy, ''Experimental study of interfacial solitary waves,'' J. Fluid Mech. **366**, 159 (1998).
[21]J. W. Rottman and J. E. Simpson, ''The formation of internal bores in the atmosphere: A laboratory model,'' Q. J. R. Meteorol. Soc. **115**, 941 (1989).
[22]J. Y. Holyer and H. E. Huppert, ''Gravity currents entering a two-layer fluid,'' J. Fluid Mech. **100**, 739 (1980).
[23]T. Maxworthy, ''On the formation of nonlinear internal waves from the gravitational collapse of mixed regions in two and three dimensions,'' J. Fluid Mech. **96**, 47 (1980).
[24]R. E. Britter and J. E. Simpson, ''A note on the structure of the head of an intrusive gravity current,'' J. Fluid Mech. **112**, 459 (1981).
[25]Y. Noh, H. J. S. Fernando, and C.-Y. Ching, ''Flows induced by the impingement of a two-dimensional thermal on a density interface,'' J. Phys. Oceanogr. **22**, 1207 (1992).
[26]R. Manasseh, C.-Y. Ching, and H. J. S. Fernando, ''The transition from density-driven to wave-dominated isolated flows,'' J. Fluid Mech. **361**, 253 (1998).
[27]B. R. Sutherland, ''Interfacial gravity currents. I. Mixing and entrainment,'' Phys. Fluids **14**, 2244 (2002).
[28]S. B. Dalziel, ''Rayleigh–Taylor instability: Experiments with image analysis,'' Dyn. Atmos. Oceans **20**, 127 (1993).
[29]S. A. Thorpe, ''Experiments on the instability of stratified shear flows: Miscible fluids,'' J. Fluid Mech. **46**, 299 (1971).
[30]G. H. Keulegan, ''The motion of saline fronts in still water,'' Technical Report 5831 Nat. Bur. Stand. Rept. (1958).
[31]C.-S. Yih and C. R. Guha, ''Hydraulic jump in a fluid system of two layers,'' Tellus **7**, 359 (1955).
[32]J. W. Rottman and J. E. Simpson, ''Gravity currents produced by instantaneous releases of a heavy fluid in a rectangular channel,'' J. Fluid Mech. **135**, 95 (1983).
[33]P. G. Drazin and L. N. Howard, ''Hydrodynamic stability of parallel flow of inviscid fluid,'' Adv. Appl. Math. **9**, 1 (1966).
[34]P. G. Drazin and W. H. Reid, *Hydrodynamic Stability* (Cambridge University Press, Cambridge, England, 1981).
[35]B. R. Sutherland and W. R. Peltier, ''The stability of stratified jets,'' Geophys. Astrophys. Fluid Dyn. **66**, 101 (1992).
[36]R. R. Long, ''Solitary waves in one- and two-fluid systems,'' Tellus **8**, 460 (1956).
[37]W. Choi and R. Camassa, ''Fully nonlinear internal waves in a two-fluid system,'' J. Fluid Mech. **396**, 1 (1999).
[38]D. J. Korteweg and G. de Vries, ''On the change of form of long waves advancing in a rectangular canal, and on a new type of stationary waves,'' Philos. Mag. **39**, 422 (1895).
[39]J. W. Miles, ''On internal solitary waves II,'' Tellus **33**, 397 (1981).
[40]M. Funakoshi, ''Long internal waves in a two-layer fluid,'' J. Phys. Soc. Jpn. **54**, 2470 (1985).
[41]M. Funakoshi and M. Oikawa, ''Long internal waves of large amplitude in a two-layer fluid,'' J. Phys. Soc. Jpn. **55**, 128 (1986).
[42]M. J. Lighthill, *Waves in Fluids* (Cambridge University Press, Cambridge, England, 1978).